Cover Page

Universiteit Leiden

The handle http://hdl.handle.net/1887/56260 holds various files of this Leiden University dissertation

Author: Antonov, Pavel
Title: Towards thermo- and superlubricity on the macroscopic scale : from nanostructures to graphene and graphite lubrication
Date: 2017-10-18

Chapter 4

Microscopic investigations of the lubrication mechanism of Diamond-Like Carbon

4.1 Introduction

Diamond-like carbon is a well-known solid lubricant coating used in a wide range of industrial applications to reduce excessive wear and friction. During the last decades, DLC coatings have revolutionized many technologies. High hardness and wear resistance [1-3,10], high thermal resistivity [e.g. 4,5], a low friction coefficient [3] and excellent chemical inertness [9] are the common properties associated with DLC films. This material has strongly proven itself in modern bearings, machine tools, gears, artificial human joints [8], etcetera. Due to its chemical inertness, DLC is widely used in vapor- and oil-lubricated contacts [1-5].

In parallel with increasing interest in its application, many research efforts are put into a fundamental understanding of the mechanism by which friction is lowered by DLC coatings with various chemical compositions. In the literature one finds different scenarios for the formation of a lubrication layer [e.g. 12-17, 31, 14]. Among these are the partial graphitization (or rehybridization) of the DLC surface [21-23], the passivation of the surface by water molecules [32] and the removal of a surface oxide [14].

Most previously published friction experiments on DLC have been conducted with uneven distributions of the loading force, at high speeds and without detailed control over the contact geometry. This makes it difficult to directly observe the dynamics and development of a lubrication layer on the studied DLC surfaces. Therefore, the formation process of the lubrication layer on DLC remains subject of debate.

In the present study, we focus on friction and wear of micropatterned DLC surfaces under ambient conditions, i.e. at room temperature in air at various levels of the relative humidity and in the absence of additional lubricants. We directly observe the formation of a layer of wear particles and show that its presence correlates with a reduction in the friction coefficient. We provide various local measurements on these particles that strongly favor the graphitization scenario, mentioned above.

4.2 Experimental

The experiments described in this chapter are performed on Dylyn DLC coatings (a-C:H)). The DLC films were deposited by magnetron sputter deposition on disk-shaped SiSiC substrates with a diameter of $5\,cm$. The DLC films are hydrogenated, because they were deposited in H gas atmosphere. The resulting H content in the films is estimated to be about $30\,at.\,\%$. The thickness of the deposited DLC films is approximately $800\,nm$. The hardness of the DLC films was measured with a nanoindenter to be $35 \pm 2\,GPa$. In order to limit the region where mechanical contact is to occur, the SiSiC substrates were micropatterned to expose three cylindrical mesas by means of plasma etching, prior to the deposition of the DLC film. The three mesas are positioned symmetrically on a $4\,cm$ diameter circle, as shown in Fig. 4.1. Each of the mesas has a diameter of $350\,\mu m$ and a height of $50\,\mu m$.

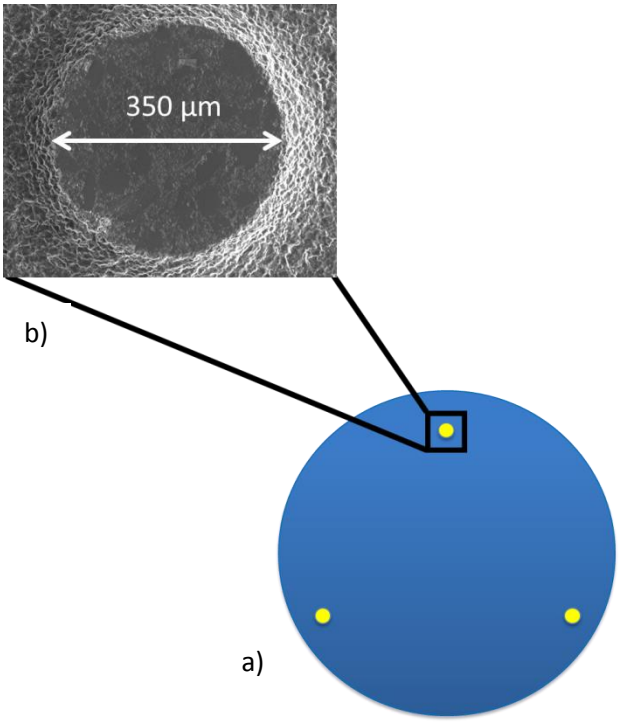

Figure 4.1. a) Principal schematic of the DLC-coated SiSiC substrate with the symmetrically positioned cylindrical mesas (yellow circles). b) SEM micrograph of one of the three mesas.

The topography of the SiSiC mesas prior to DLC deposition exhibits relatively large polished plateaus (domains) with an average roughness of $10 \div 15\ nm$. After deposition of the DLC coating, the resulting surface roughness is nearly unchanged. A typical AFM height map of the plateaus shows long scratches and local pits, originating from the final, fine-grain polishing treatment of the substrate (Fig. 4.2).

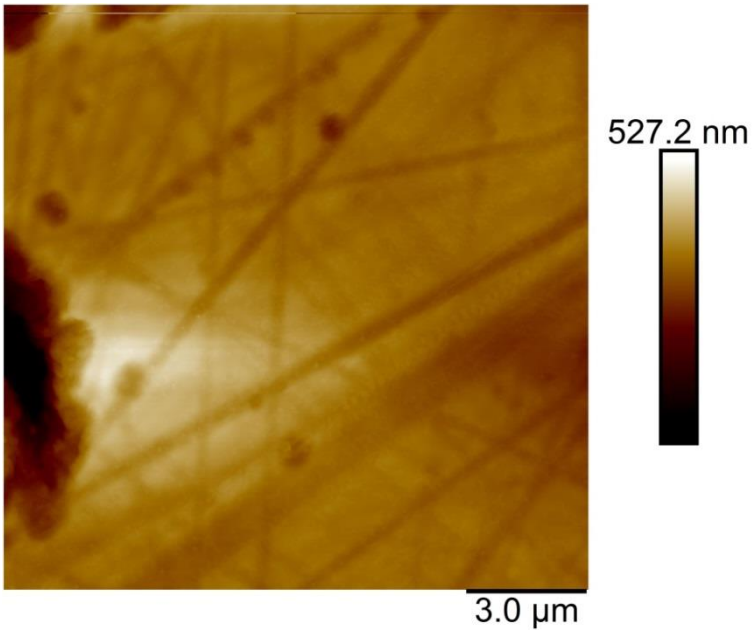

Figure 4.2. $15x15\ \mu m^2$ *AFM height image of the surface of a flat plateau on a DLC-coated mesa. The surface is composed of flat areas with scratches and pits, separated by deeper parts. An average roughness of the flat plateau is* $10 \div 15\ nm$*. Areas between the plateaus are lower than the plateaus.*

Figure 4.3 shows two optical micrographs of a DLC-coated mesa, taken with a Bruker Contour Elite 3D Optical microscope. The two micrographs represent an overview over one entire mesa and a local region of the mesa surface at higher magnification. Again, we recognize the flat plateaus and we see that they are distributed densely over the mesa and that they cover most of the surface. Consistent with the AFM image of Figure 4.2, the optical micrographs show that the regions between the plateaus are all lower than the plateaus themselves.

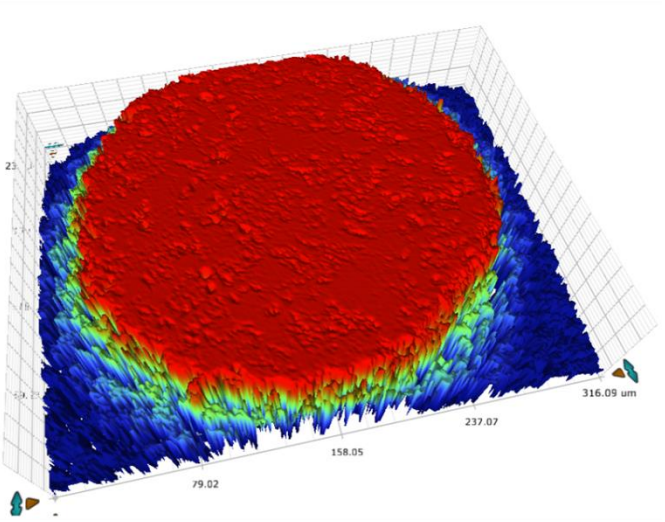

a)

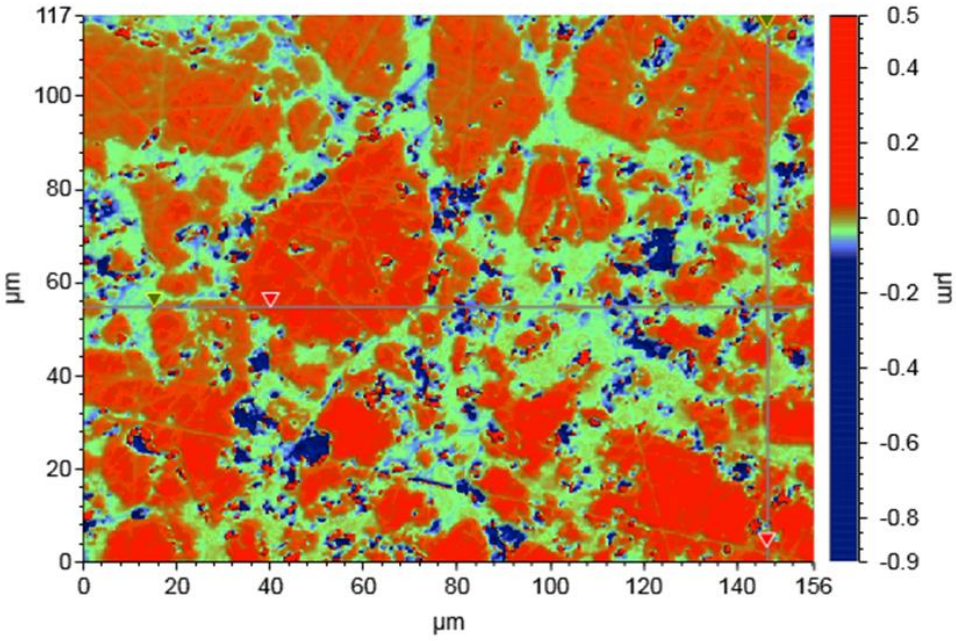

b)

Figure 4.3. 3D optical micrographs of a DLC-coated mesa. a) complete mesa; b) representative, local area of $156 \times 117\ \mu m^2$ *on the mesa.*

As a counter-surface for the friction experiments we use 2 inch diameter Si(100) wafers with a thickness of $250\,\mu m$. Typically, these wafers are mildly warped. Using an interferometer, we measure the out-of-plane deformation to be 1 to $5\,\mu m$ across the wafer diameter. The weight of a wafer is approximately $12 \pm 0.15\,mN$. The precise value is measured for each separate wafer with a sensitive scale, prior to each friction experiment. Most experiments are conducted with untreated wafers supplied by Si-Mat Company [48], for which the surface is known to be covered by a native oxide, SiO_2, with a typical thickness of $2 \pm 0.5nm$. All friction experiments were conducted using a polished side of the Si wafers, which roughness was measured to be $0.9 \pm 0.2\,nm$ (Fig. 4.4). Some of the wafers are covered with a DLC coating, giving us the possibility to create two different tribological pairs, as will be discussed later.

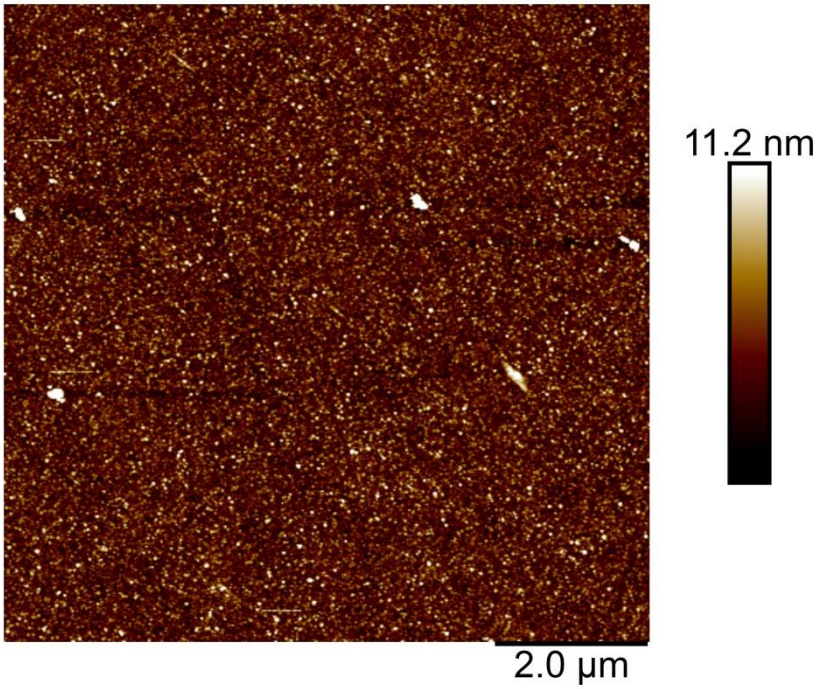

Figure 4.4. $9 \times 9\ \mu m^2$ *AFM height image of a polished side of the Si wafer.*

Static and dynamic friction forces are measured with a friction force microscope in the form of a Bruker Universal Mechanical Tester (UMT-1). The

microscope is equipped with a sensitive, low-noise, three-dimensional strain-gauge force sensor that has a resolution of $1\ \mu N$ for both components of the lateral force and for the normal force. The sensor can be operated in a force range from approximately $10\ \mu N$ to $12\ mN$. The maximum force value the microscope is able to measure is set by the mechanical strength of the sensor components. As a 'probe' we use a rectangular aluminum block attached to the sensor. The dimensions of this block are $5 \times 5\ mm^2$ parallel to the (horizontal) sliding interface and $15\ mm$ in height. A photograph of the measurement system and a schematic picture of the geometry are presented in Figs. 4.5 a and b. The aluminum block is used to push the silicon wafer back and forth along the micropatterned substrate, simultaneously measuring the lateral forces, exerted on the block.

In the UMT-1 setup, the three-mesa substrates are mounted on a positioning stage beneath the sensor. The stage can translate along the two lateral directions, X and Y, while the force sensor can translate along Z, all using built-in stepper motors with an accuracy of $100\ nm$. The stage can rotate (Θ) with an accuracy of $10\ nrad$. A very important question is how to properly align the contacting surfaces with respect to each other. We achieve the best possible alignment without any mechanical adjustments by simply positioning the slider (i.e. the silicon wafer) onto the substrate (DLC-coated SiSiC) under the force of gravity. The silicon wafer freely rests on the DLC-coated mesas with a normal force dictated by its own weight ($12\ mN$). Friction forces are measured by using the aluminum block on the force sensor to apply tangential forces on the flat side (marker plane) of the wafer. In this way, no torque is exerted on the wafer, which therefore remains aligned and in proper contact with the substrate throughout the entire sliding experiment. The normal force can be increased by adding calibrated weights on top of the wafer.

Some experiments are conducted in reciprocating mode, using a sequence of displacements of the Si wafer back and forth along the sliding direction. This enabled us to observe run-in behavior of the DLC films without limitations on the total sliding distance. We solve this problem by means of gluing two square pieces of silicon wafer, each with dimensions of $0.5 \times 0.5\ cm^2$, on top of the unpolished side of the sliding Si wafer. They are positioned accurately with respect to the center of the wafer and aligned with respect to each other. Therefore, the aluminum block of the UMT-1 setup can be placed between them and sequentially moved back and forth to conduct the measurement of the lateral force. The

resulting value of the lateral force is found to be in good agreement (absolute difference up to 5%) with the value measured by pushing against the side of the wafer, as described above. The additional normal load due to the square blocks is $1\,mN$. Unfortunately, in some experiments we recognize that even a slight asymmetry in the gluing of the two auxiliary Si pieces with respect to the center of the sliding wafer results in differences between the values of the lateral forces measured in the forward and reverse sliding directions. On the other hand, differences of this type are fully systematic and remain unchanged during the sliding experiments. The measurement in Fig. 4.12 demonstrates such a slight asymmetry between the lateral force values for sliding in the two opposite directions.

With this experimental arrangement, a friction measurement with the UMT-1 setup is composed of a sequence of short, unidirectional sliding trajectories of typically $1\,mm$ sliding distance. At the end of each trajectory, the sliding direction is reversed. We plot the sequence of positive and negative lateral forces that are measured during a series of forward and reverse sliding trajectories into a single plot, from which we can see the full history of the friction force over the sequence.

Friction experiments are conducted at temperatures of $21 \div 25°C$. The atmosphere in the UMT-1 chamber can be controlled by passing a mixture of dry nitrogen gas and moist air through it. In this way, the relative humidity (RH) in the chamber can be varied between 1% and 90%. The RH was measured close to the substrate position with a hygrometer, Vaisala HM40 [55].

Additional topography and friction measurements on nano- and microscopic levels are performed with an Atomic Force Microscope (AFM) Dimension Icon (Bruker). Friction force measurements with this AFM are all carried out with Bruker silicon nitride V-shape probes DNP-10 with normal spring coefficients of 0.05 to $0.2\,N/m$.

We inspect the surfaces of the wafer and the mesas at various stages in our experiments with Scanning Electron Microscopy (SEM) and Energy Dispersive X-Ray Spectroscopy (EDX), using a FEI Verios. Micro-Raman Spectroscopy is performed on Renishaw Raman microscope, with a laser wavelength of $514\,nm$ and an exceptionally small laser spot size of $500\,nm$, enabling us to acquire local spectra on specific structural features.

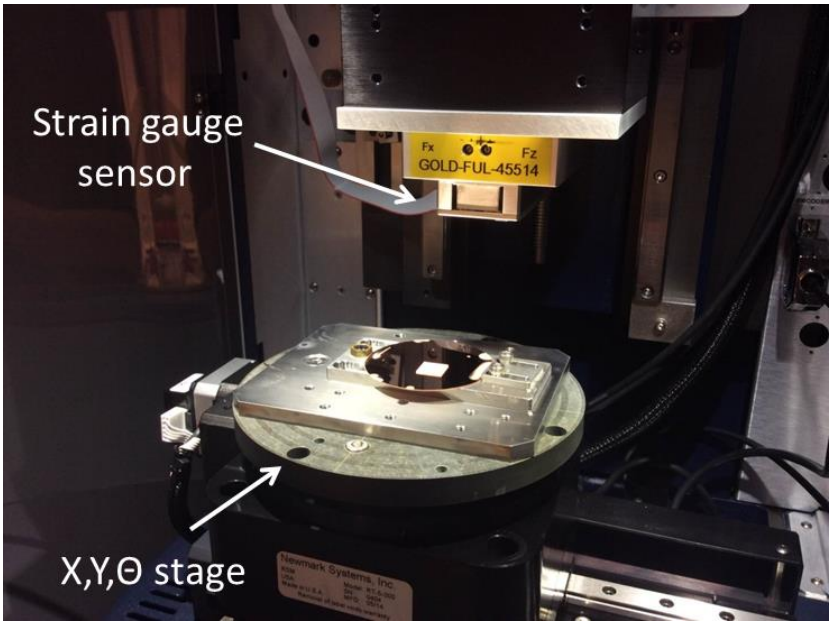

a)

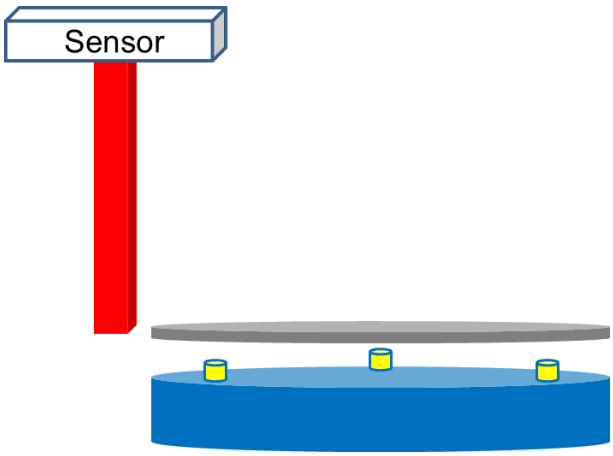

b)

Figure 4.5. a) Photograph of the Bruker Universal Mechanical Tester (UMT-1) used for most of the friction experiments in this chapter. Indicated are the translation-rotation stage on which the three-mesa substrate is mounted and the strain-gauge force sensor that is used to exert the lateral force on the sliding wafer. b) Schematics of the experimental setup, with the three mesas (yellow), the silicon wafer (grey) and the aluminum block (red) that is connected to the force sensor.

4.3 Results and discussion

The first set of experiments was conducted with pristine silicon wafers as the counter-surface. As the wafers are nearly flat, they provide a well-defined interface geometry with the DLC-coated mesas. This geometry is dictated by the detailed pattern of asperities on the three mesas and remains unchanged, irrespective of the sliding direction and speed and of changes from one silicon wafer to another.

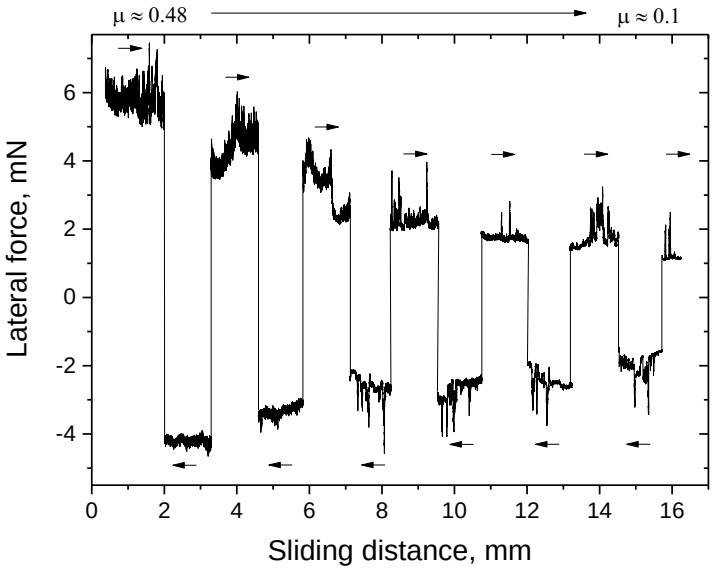

Figure 4.6. Initial reciprocating friction measurement with a silicon wafer on a 'fresh' DLC-coated three-mesa sample. The rapid reduction in lateral force illustrates the run-in process. Normal load $13\ mN$*, velocity* $10\ \mu m/sec$*, relative humidity* 45%*. Black arrows point at the sliding direction.*

Each friction experiment with a new DLC coating began with a so-called 'run-in' period, during which the friction forces started out high and gradually decreased to low and stable values. Figure 4.6 illustrates the run-in process for a new silicon wafer sliding for the first time on a substrate with freshly prepared DLC-coated mesas. After a total sliding distance of only $10\ mm$, the friction force is decreased by approximately a factor 5. This indicates that the contacting interface has undergone a dramatic change that causes excellent lubrication. We ascribe our

short run-in distance to our special geometry in which the sliding, flat silicon wafer makes contact continuously with the same asperities, which leads to their rapid modification.

Directly after the first friction measurements and total sliding distance of 15 mm, the surfaces of both the silicon wafer and the mesas were inspected with SEM and EDX in search for structural or compositional changes. The SEM images show that the mesas get decorated by third-body elements. Figure 4.7 shows a comparison of two similar regions of a DLC-covered mesa before and immediately after the run-in. Comparison of precisely the same locations prior to and after the first sliding experiment is rather difficult, because one should know beforehand at which exact location on the mesa the third-body particles will be formed first. In Fig. 4.7b one can see substantial numbers of flakes and particles distributed in depressions between the flat plateaus. The difference in contrast (i.e. in electron work function) between the SEM images in Figs. 4.7a and 4.7b indicates physical/chemical changes occurring in the top layer of the DLC during the initial sliding. We will return to this in the Results and Discussion section.

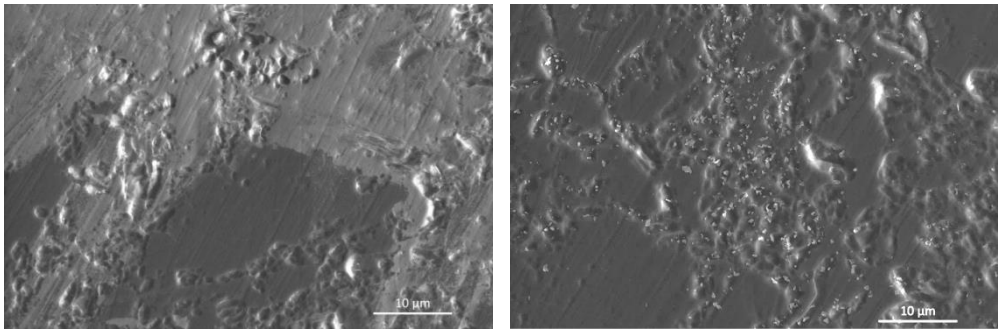

a) b)

Figure 4.7. Comparison of SEM micrographs of nearly the same area of a DLC-coated mesa before (a) and after the run-in process (b) of Fig. 4.6. The arrow in panel (b) indicates one of the numerous third-body particles that decorate the mesa after the first sliding contact. Higher-resolution images of these particles are shown in Fig. 4.8.

Upon closer inspection with EDX it appears that not one but two types of new species can be identified. The first type, Fig. 4.8a, is formed by flake-like silicon particles. They form a wear product of the silicon wafer, due to its contact with the relatively sharp nano- and micro-asperities on the mesa surface. Figure

4.8b shows another location where debris has developed, the EDX spectrum showing mostly carbon and no silicon. These carbon-based flakes must be worn off from the DLC surface due to the high local stresses during the initial sliding. They are typically in the order of 0.5 μm diameter and 10 to 25 nm thick. Interestingly, some of these particles show a different contrast in the SEM images, which indicates a difference in electronic structure with respect both to the substrate and to the other particles. We will return to this observation later. According to our SEM analysis, both types of flakes can easily shear across the surface, changing their locations during the sliding of the silicon wafer on top. We conclude this, based on the absence of some of the particles in the SEM images from the DLC mesa after the sliding experiments. We find, however, that they are not likely to be transferred to the silicon surface, which shows that their adhesive interaction with the DLC surface is significantly stronger.

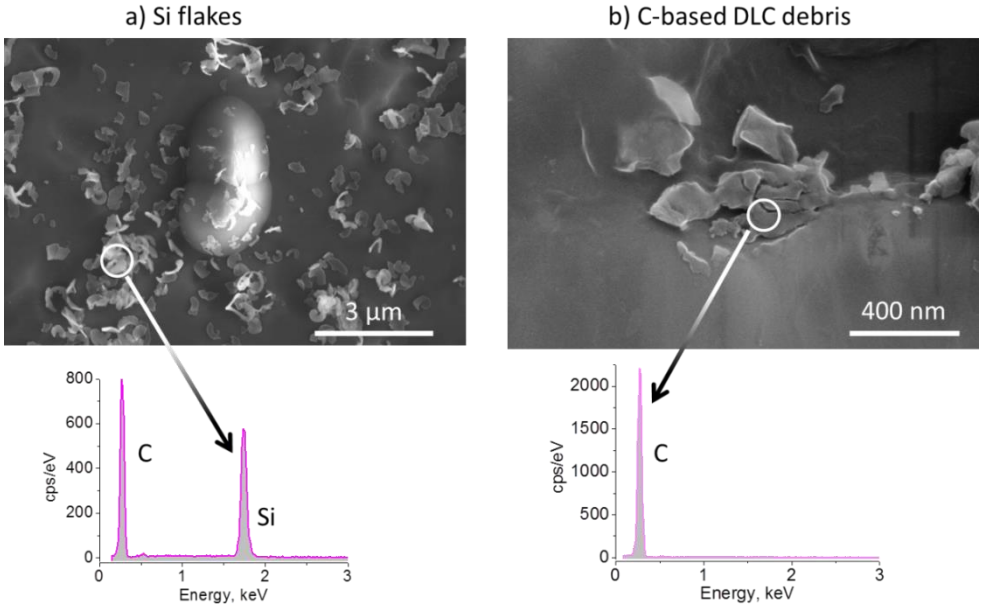

Figure 4.8. SEM images and EDX spectra on the DLC-coated mesas after the run-in process: a) silicon flakes, b) carbon-based flakes. EDX spectra are measured at the locations marked with the white circles.

In contrast with the carbon-based flakes, the silicon flakes are generated primarily within the first sliding cycles. Indeed, one can assume that during the run-in phase the silicon wafer makes direct mechanical contact only with a few microscale asperities on each of the three DLC-coated mesas. The resulting contact stresses may easily reach tens of GPa, thereby exceeding the fracture stress of bulk silicon is 10 GPa in humid environment [44]). After the run-in process, contact stresses are lower and do not result in fracture of the silicon wafer anymore, even though they may remain significant – a point that will be of qualitative importance later in this chapter.

Hand in hand with the deposition of silicon flakes on the DLC-coated mesas, wear tracks are formed on the silicon wafer, in the areas where the wafer was in direct contact with the DLC mesas. Optical microscopy images (Fig. 4.9) show scratches on these locations. The total length of each wear track is equal to the sliding distance covered during the run-in phase. SEM images show two types of wear tracks, one type resulting from a continuous, smooth cutting through the silicon (Fig. 4.10a), while the other indicates a repeated chipping off (Fig. 4.11b),

reminiscent of stick-slip motion. Both types show the removal of silicon from the wafer, so that both should be expected to result in the supply of silicon flakes to the sliding interface.

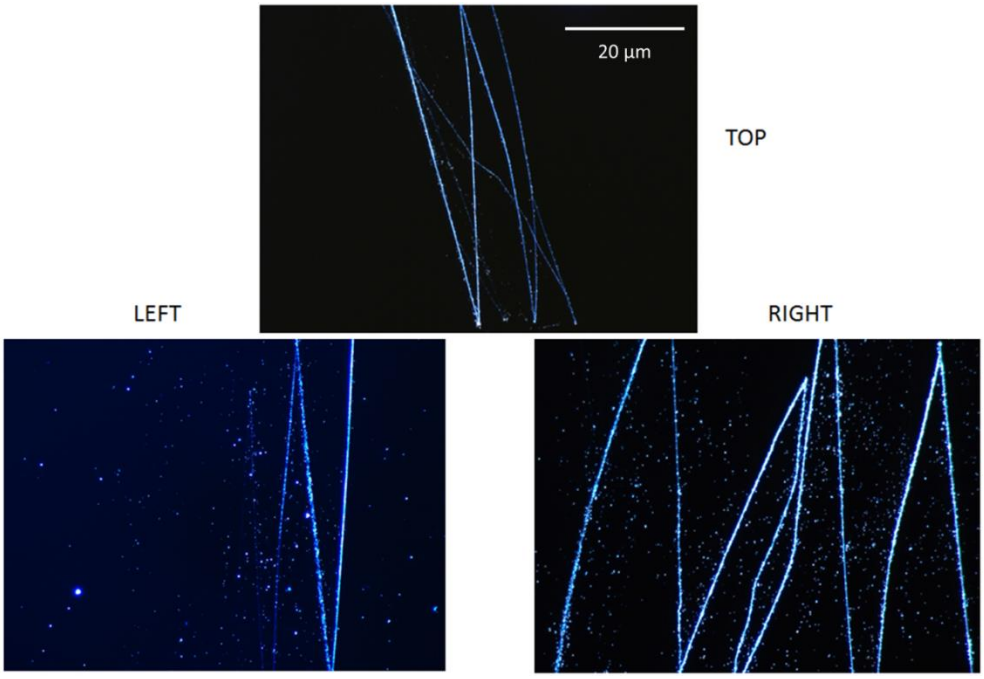

Figure 4.10. Optical micrographs (dark field) of the wear tracks formed on the sliding surface of the silicon wafer during the run-in process on the DLC-coated three-mesa surface. Note the high density of silicon particle debris along each wear track.

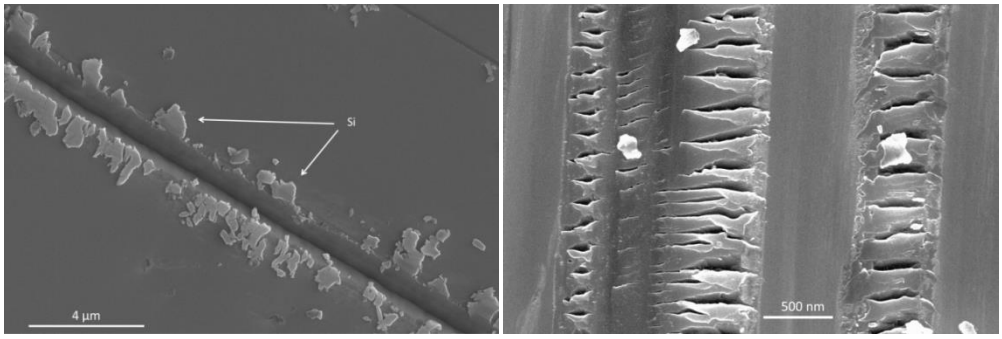

a) b)

Figure 4.11. SEM micrographs of wear tracks on the silicon wafer: a) a small-scale region with a continuous cut through the silicon surface; b) a large-scale image showing the result of a 'stick-slip'-type sequence of chipping events.

Once the run-in is complete and the friction force is low, any subsequent sliding of the wafer does not lead to any further wear of the silicon wafer. When we replace the first silicon wafer, used for running in, by a fresh wafer, the friction force remains low (Fig. 4.12) and the new wafer is not scratched. Note, that there is a consistent absolute difference between the values of the lateral force measured during sliding from right to left and from left to right. This is presumably due to slight difference in position of the Si blocks placed on top of the wafer with respect to its center, as discussed above in Experimental. For this reason, here we show an average value of the friction coefficient of the corresponding reciprocating paths $< \mu >$.

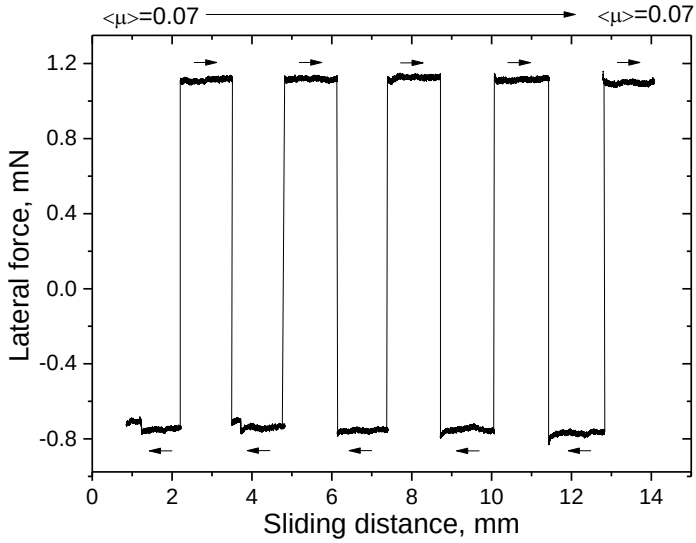

Figure 4.12. Reciprocating friction measurement performed with a fresh silicon wafer on a DLC-coated substrate, after the substrate had been run in with a separate silicon wafer, similar to the friction sequence displayed in Figure 2. Normal load 13 mN*, velocity* 10 $\mu m/sec$*, relative humidity* 45%*. Black arrows point at the sliding direction.*

During consistent inspection of the fixed locations on the DLC mesas which contain Si flakes we observed that Si flakes may move and disappear from their original position after sliding of the wafer. At the same time, we don't find them being transferred back to the Si wafer surface. We may conclude that the silicon flakes have significant mobility at the interface. This is surprising if we assume that

they exhibit similarly strong wetting by water as the (oxidized) surface of the silicon wafer [49]. In contact with the wafer under ambient conditions, the silicon flakes should then be pinned to the wafer through the formation of capillary water bridges. But as we find that they are relatively free to slide, whereas we have not observed the transfer of silicon flakes back from the DLC surface to the silicon wafer, we have to conclude that the silicon flakes, or at least their surfaces, are chemically modified. We will return to this point later in this chapter.

The dependence of the friction force on the applied normal load is measured to be close to linear for normal load values up to approximately $F_N = 40\,mN$. This can be recognized in Fig. 4.13, in which we plot the coefficient of friction (COF), defined as the ratio $\mu = F_F/F_N$ between the friction force and the normal load and where the friction force is equal to the average lateral force $F_F = \overline{F_L}$. Up to $F_N = 40\,mN$, the COF is more or less constant.

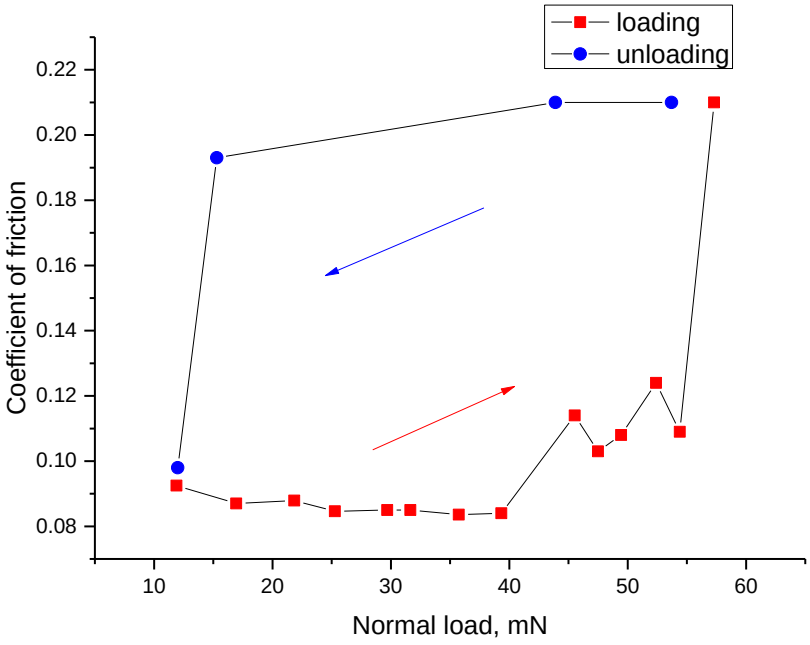

Figure 4.13. Dependence on normal load of the friction coefficient for a silicon wafer on a DLC-coated substrate. The red curve represents measurements during the loading phase, i.e. while the normal load is gradually increased. The blue curve shows measurements during unloading. The weight of the silicon wafer was $12\,mN$. *The*

normal load was varied by means of adding extra weight on top of the silicon wafer. Relative humidity 45%, *temperature* $23°C$.

The high lateral mobility of the silicon particles was found only within a certain range of normal loads. When the normal load was gradually increased beyond $40\ mN$ (red curve in Fig. 4.13), we observed a rapid increase of the friction coefficient. For $F_N \geq 55\ mN$, the friction force even reached the maximum value of $12\ mN$, at the limit of the operational range of the force sensor. In fact, the values of the friction coefficient in Fig. 4.13 higher than 0.2 are lower estimates. Along the blue curve, we gradually decreased the normal load. The wafer could slide again after we reduced the normal force to $F_N = 15\ mN$. We assume that the changes in friction coefficient are due to the pinning of the Si and DLC particles on the DLC film at high normal loads. When the load is reduced sufficiently, the particles, presumably, de-pin and regain their ability to shear across the surface. This phenomenon causes hysteresis in the loading-unloading cycle, when we load beyond a critical level. Along with this assumption, we cannot exclude another scenario which takes into account contact stresses on the surface of the silicon wafer. Let's assume that the real contact on each DLC mesa takes place only via small number of third-body particles (and asperities) with sub-micron size distribution. As discussed above, at a normal load of $F_N = 12\ mN$ after the run-in process, the Hertzian contact stresses could reach a level up to several GPa, which is roughly comparable with the ultimate strength of bulk silicon. Hence at a 5 times higher normal load (Fig. 4.13), one should already expect a gradual fracture of the silicon surface in places of real contact. As follows, in order to rejuvenate sliding motion and reach the original friction coefficient, one should decrease the normal load.

In order to demonstrate that silicon particles only help to bring down the COF by mechanical filling-in and shielding of the DLC surface, we conducted an experiment in which we partially removed them by cleaning the mesa structure after which we measured the friction force again. The cleaning was conducted in an ultrasonic bath with n-octane for $15\ min$ at $20°C$. n-Octane as a non-polar solvent increases the probability for the particles to come off the surface. In fact, using of a polar solvent (e.g. isopropanol) didn't result in removing of any particles. We assume the reason for this is an interaction of polarized solvent

molecules with the surface of the DLC film and the particles. Due to a strong dipole moment acting between them, the particles had in the particular case lower probability to come off. Interestingly, only silicon flakes were removed in this way, while C-based particles could not be removed from the mesa surface. Figure 4.14 represents SEM images of a local area on the DLC surface before and after cleaning of the DLC substrate following the proposed above procedure.

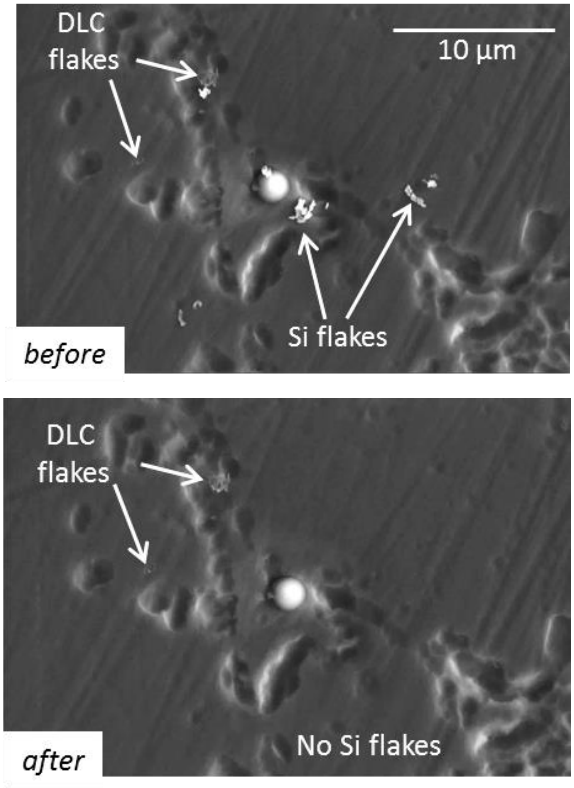

Figure 4.14. Example of the same local area on a DLC-coated mesa before (a) and after (b) ultrasonic cleaning with n-octane. Note that most of the silicon flakes created around an asperity are gone after cleaning, while the DLC flakes remain on their original positions.

In Fig. 4.15 we show a friction measurement with a fresh silicon wafer against a DLC-coated three-mesa substrate, directly after the cleaning procedure described above, in which the silicon flakes were removed. While the initial value of the COF is much lower than the starting value observed at the first run-in of the DLC coating (Fig. 4.6), the COF starts out higher than its value after that run-in, but prior to the removal of the silicon flakes. A new run-in episode is required to reduce the COF again. Note that in this process the 'noise' on the measured lateral force is high initially and that it is reduced nearly to zero during the run-in phase. After this re-run-in measurement, SEM images showed new silicon flakes at locations next to asperities and in relatively flat areas, where such flakes had been absent after the sonication. We see that the presence of the silicon flakes correlates with a modest reduction in the COF and with the suppression of the fluctuations in the lateral force.

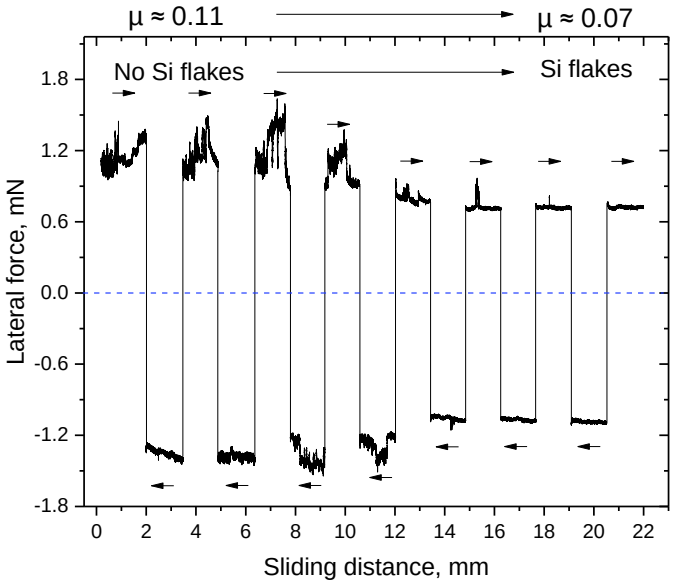

Figure 4.15. Friction measurements between a fresh silicon wafer and a DLC-coated three-mesa substrate, immediately after 'cleaning' the substrate in an ultrasonic bath with n-octane. SEM-images show that initially no flakes were present. At the end of the test a small number of new silicon flakes were observed. Normal load 13 mN*, velocity* 10 $\mu m/sec$ *and relative humidity* 45%*. Black arrows point at the sliding direction.*

In order to completely exclude the influence of the silicon flakes on the lubrication process, in the next set of experiments we used as a counter-surface a silicon wafer coated with DLC, i.e. with the same type hydrogenated coating as the three mesas over which it was forced to slide. The thickness of the DLC coating on the silicon wafer amounted to $800 \pm 10\ nm$. AFM topography measurements on the DLC-surface show that it has a local roughness of $1.1 \pm 0.2\ nm$, which is similar to the roughness of the underlying silicon surface (Fig. 4.16). Therefore, the geometrical simplicity is conserved of a nominally flat counter-surface sliding over the rough surface landscape of the three mesas.

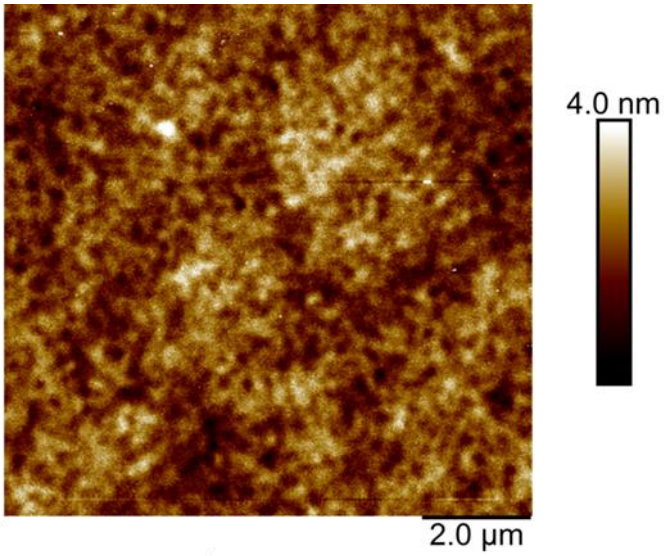

Figure 4.16. AFM height measurement on the DLC-coated silicon wafer. The root-mean-square (rms) roughness equals $1.1 \pm 0.2\ nm$*, which is similar to that of the silicon wafer.*

Figure 4.17 presents a friction measurement with the DLC-coated silicon wafer against the DLC-coated mesas. During a rapid run-in process, the COF decreases during the first millimeters of sliding, reaching an average final value of 0.09 ± 0.01 and remains almost unchanged even at longer sliding distances ($> 10\ mm$).

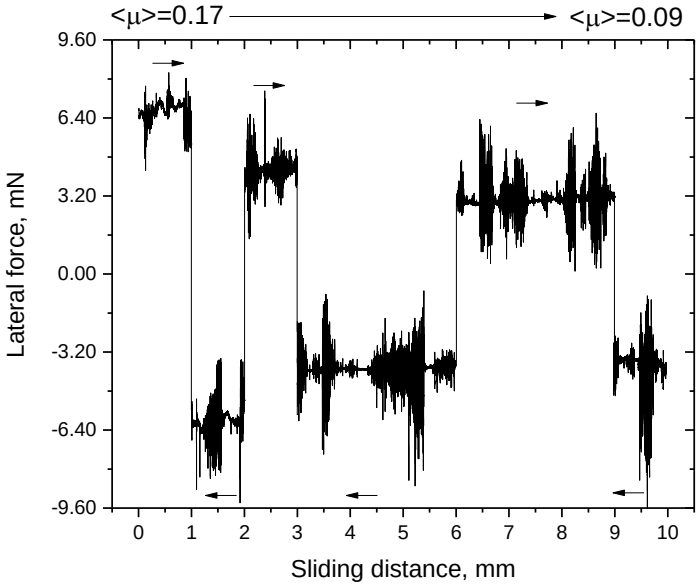

Figure 4.17. Friction coefficient during the run-in process of a DLC-coated silicon wafer against a DLC-coated three-mesa substrate. Normal load $35\ mN$*, velocity* $10\ \mu m/sec$ *and relative humidity* 45%*. Black arrows point at the sliding direction.*

In the experiments with an uncoated silicon wafer sliding over the DLC-coated mesas, carbon-based particles were generated in the form of submicron flakes. In the present case, with DLC-coated surfaces sliding over each other, we first observe the formation of rather large particles, with diameters up to several micrometers (Fig. 4.18), which we ascribe to the high interfacial hardness. They originated mostly from the substrate and only minor wear loss was observed on the DLC-coated silicon wafer. Only after sufficiently long sliding distances, these particles decreased in size, probably due to the milling effect between the contacting regions. Presumably, the milling and shear sliding of the loos particles causes the noise in the lateral force signal, observed in this experiment. The final average size of most particles does not exceed the interface roughness of approximately 10 to 50 nm, dominated by the roughness of the mesas. Though minor amount of the particle still have the size larger that the interface roughness, therefore the noise remains present even at longer sliding distances ($> 10\ mm$).

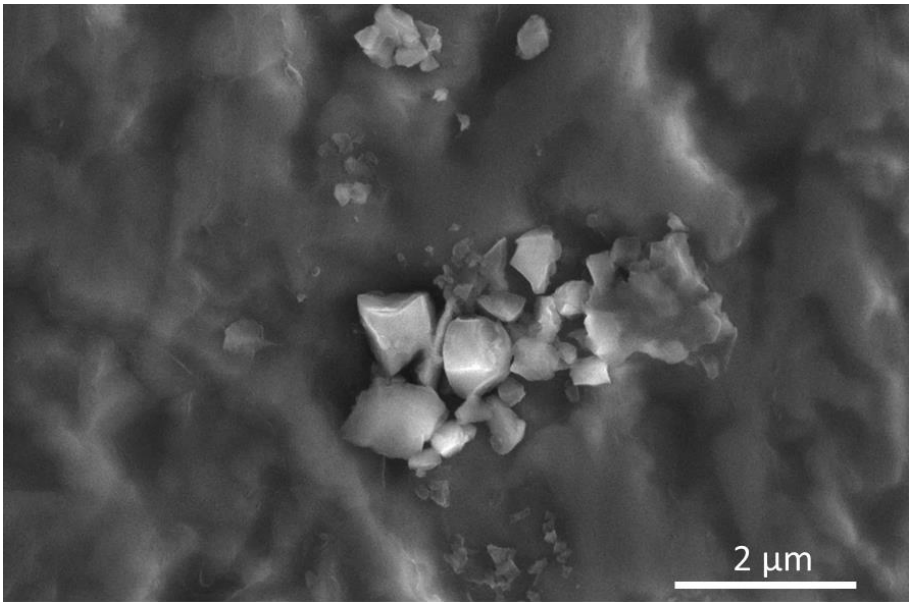

Figure 4.18. SEM micrograph of particle debris formed during the run-in period (after the first 3 mm of sliding in Fig. 4.10) at the interface between two DLC-coated surfaces.

Similar to the silicon-against-DLC experiment, the carbon-based particles formed in the DLC-against-DLC experiment could not be removed by means of ultrasonic cleaning in n-octane, following the method described above. As long as these carbon-based flakes are present on the DLC mesa surface (and also on the sliding surface of the DLC-coated silicon wafer) and the majority of protruding asperities are removed, the DLC surface is in its 'self-lubrication' regime. The low friction coefficient is conserved if the counter-surface is replaced with a different one. For example, if after the run-in process, the DLC-coated silicon wafer is replaced with a new, uncoated silicon wafer, the COF remains nearly unchanged and no further run-in behavior is observed (Fig. 4.19). Also, no scratches are formed on the silicon and no material is transferred from the silicon wafer to the DLC-coated mesas.

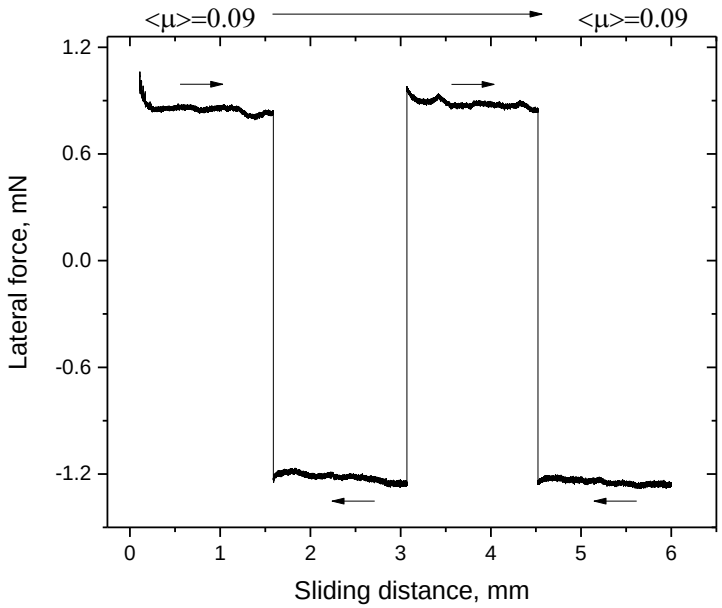

Figure 4.19. Reciprocating friction measurement with a fresh, uncoated silicon wafer sliding over a DLC-coated three-mesa substrate, after this substrate had been run in against a DLC-coated silicon wafer. Normal load $13\ mN$*. Reciprocating speed* $10\ \mu m/sec$*. Relative humidity* 45%*. Black arrows point at the sliding direction.*

Firstly, observed mobility of the Si flakes might tempt to idea that their surface got wrapped with a thin layer of carbon material transferred from the DLC surface during their initial shear. Similar scenarios of lubrication due to formation of onion-like structures on diamond particles between graphene and DLC surface were suggested earlier [18,19]. A micropillar geometry gives us an opportunity to look at individual particles in the transfer layer. Therefore we put an effort to characterize individual silicon and C-based flakes with micro-Raman spectroscopy, to find out whether above mentioned scenario could be applicable in the particular case. The measurements were performed on the silicon particles didn't reveal any structural changes: unfortunately, due to a strong background signal from DLC no significant correlation of graphitic structure present on the silicon particles was found, though a Raman laser spot was as small as $500\ nm$ in diameter. A typical Raman spectrum on the silicon particle on DLC surface is presented on Fig. 4.20.

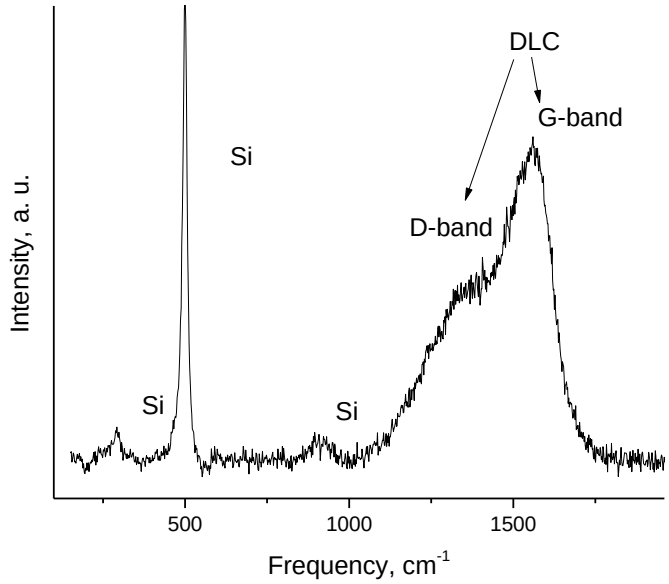

Figure 4.20. A typical Raman spectrum measured on a single silicon flake laying on the DLC surface. A part of the spectrum from $\sim 1000\ cm^{-1}$ *to* $\sim 1750\ cm^{-1}$ *is due to the background signal from DLC.*

Secondly, our observations indicate that the surface of the carbon-based particles that are formed during the run-in phase, has undergone a dramatic structural or compositional change. This is consistent with many previous studies [e.g. 13, 21-23]. The most popular scenario is that the density of carbon atoms involved in sp^2 bonding configurations would be increased at the surface of the DLC particles that are sheared off from the DLC coating. This increase in sp^2 signature would correspond to a local surface conversion from the original, hard diamond-like carbon phase, with sp^3 bonding character, into a graphitic carbon network. Such a conversion is possible under sufficiently high local pressures and shear stresses. Many spectroscopic studies demonstrate agglomeration of converted carbon based particles along the wear tracks on the studied samples [e.g. 22, 50]. For the hydrogenated DLC, this process should also be accompanied with some hydrogen release from the structure and a resulting lattice relaxation. Indeed, the friction between diamond surfaces has been measured to be extreme [51]. In contrast, the friction between graphite surfaces can be vanishingly low [35]. The

combination of high stiffness within each graphite sheet and the weak Van der Waals bonding between the sheets, makes it relatively easy to shear graphite or graphene sheets over each other, particularly when they are azimuthally misaligned [35]. We have to realize that the proposed diamond-to-graphite conversion should be expected to take place only very locally, where direct mechanical contact generates sufficiently high pressures. The lubricating carbon-based particles could be decorated by graphitic carbon only over a small fraction of their surface. This makes it very difficult to prove experimentally that such a structural transformation is indeed taking place and that it is indeed responsible for the strong reduction in measured friction forces.

In order to investigate the possible structural transformation of the carbon-based particles, we performed micro-Raman spectroscopy. Special in these measurements was the use of a relatively small laser beam spot, enabling us to acquire spectra completely on a single particle or, for comparison, on the DLC areas between the particles. In order to ensure that the Raman spectrum for the particles was obtained exclusively on particles, we selected particles for this analysis with lateral dimensions larger than $800\,nm$. In Fig. 4.21, we compare a spectra in the frequency range between 900 and 1800 cm^{-1} on a pristine DLC area on one of the mesas with a spectrum on a single carbon-based particle. The characteristic bands for DLC are around $1360\,cm^{-1}$ ('defect' or D-band) and $1550\,cm^{-1}$ ('graphite' or G-band) and overlap. These bands originate mainly from sp^2-bonded carbon clusters. Their intensity ratio I_D/I_G, their widths and precise peak positions are all sensitive to details of the bonding configuration and thus to possible structural changes, e.g. from sp^3 to sp^2. We used a standard Gaussian peak fitting method, which is described in detail in e.g. [24-28, 39], in order to process the acquired Raman spectra and analyze the D and G bands independently, in terms of their intensities, positions and full widths at half maximum (FWHM). A combination of these parameters serves as a measure for the relative amount of sp^2-bonding [27, 29, 30, 39]. Comparing Figs. 21b (particle) and 21a (DLC), we observe the following:

1) a significant increase of the I_D/I_G ratio on the particle with respect to the pristine DLC, from 0.56 to 0.91. Note that this is primarily due to a significant increase of I_D, while I_G remains almost constant;

2) a shift of the G band position towards higher frequency, from 1553 to 1560 cm^{-1};

3) no shift of the D peak;

4) a narrowing of the FWHM of both the D and the G band.

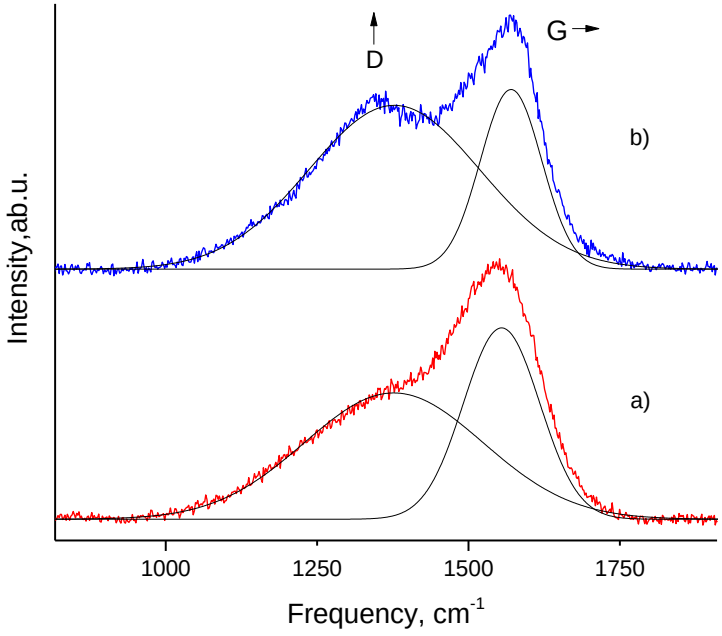

Figure 4.21. Comparison of the Raman spectra of the pristine DLC surface (a) and on top of a wear particle of the DLC (b). The black inner lines illustrate the Gaussian decomposition into D- and G-bands. The spectra are offset vertically for clarity.

We note, that the penetration depth at 514 nm wavelength of the laser can be as large as 700 nm [53]. Therefore, in all measured spectra only a part of the signal corresponds to light interaction with the surface, while the rest is due to interaction of the excitation laser light with the bulk material. The Raman spectra suggest that the investigated particles contain a relatively high number of sp^2-bonded carbon atoms in comparison with the DLC film. The particles originate from the asperities that had undergone the highest mechanical stresses due to the uneven distribution of normal load during the run-in phase. In turn this induces local atomic stresses in

the DLC, followed by transformation of metastable sp^3-bonded clusters into to more stable sp^2. In the presence of adsorbed water, the dangling bonds on the sp^2-clusters should be passivated, similar to the situation for graphite [54]. Without the dangling bonds, the sp^2-clusters can act as an efficient lubricant. Carpick *et al.* have recently shown that in addition to some rehybridization from sp^3 to disordered sp^2-bonding in non-hydrogenated amorphous carbon and ultra-nanocrystalline carbon, an essential ingredient in the solid-lubrication mechanism of amorphous carbon is the passivation of active sites (dangling bonds) with OH and H, formed due to dissociation of adsorbed water [15]. They have concluded this, based on near-edge x-ray adsorption fine structure (NEXAFS) spectroscopy measurements on the wear tracks. In our case of hydrogenated DLC, both processes play a positive role in lubrication of the solid interface. On the one hand, the increased number of sp^2-bonded carbon clusters reorganizes the particle surface and also results in rupture of C-H bonds and increasing density of carbon dangling bonds, thus increasing the surface energy. C-H bonds are known to break mechanically by the high shear stresses that develop locally during sliding [52]. On the other hand, newly created active sites on the particles get immediately passivated with water from the environment, bringing down the friction coefficient [47]. The rest of the substrate remains enriched with H, which locally passivates all dangling bonds and prevents water from adsorbing [32-34]. Also, the Raman spectrum measured on the DLC surface next to the particles does not show any sign of increasing amount of sp^2 clusters. Therefore, we conclude that the lubrication is mainly due to hybridization and/or passivation mechanisms on the wear particles, rather than a transformation of the entire DLC substrate. We defer the discussion of the dependence of friction on the relative humidity to the next Chapter, where we present experimental data.

The change in electronic structure, associated with the increase in the proportion of sp^2 bonded surface atoms on the studied particles, should be expected to cause a change of contrast of the particles in the SEM observations, as mentioned above. The reason for this is that the electronic changes should be accompanied by changes in the work function and, hence, in the secondary electron emission coefficient. A change in contrast between sp^2 and sp^3 clusters has been reported before in Transmission Electron Microscopy observations [46].

One important observation from this work is that even in our special geometry, in which the roughness is fully concentrated on one of the two contacting surfaces and the asperities on that surface seem more or less fixed in location, all major transformations of the DLC film are very local and the final contact geometry is strongly dominated by the third bodies that are formed during the initial, run-in phase. In this extremely heterogeneous geometry, the commonly used term 'wear track' is not appropriate [6, 28]. We inspected the local variations in frictional behavior on the mesa surface with AFM. Figures 4.22 a and b present maps of the friction and height of the same local region on the DLC film. The combination of these images shows that some of the highest locations exhibit relatively low friction levels, compared to the lower regions that did not experience sliding contact with the counter surface. The latter means that due to the relatively high local contact pressure, the highest regions have undergone physical or chemical changes that cause the lowering of friction on them. Ahn et al [40] studied phase images with AFM [42, 43] on DLC wear tracks. They revealed a significant inhomogeneity of the wear track across the sliding direction and reported a lower elastic modulus on the highest asperities. The latter was associated by them with a transition of the diamond-like structure to a graphite-like structure.

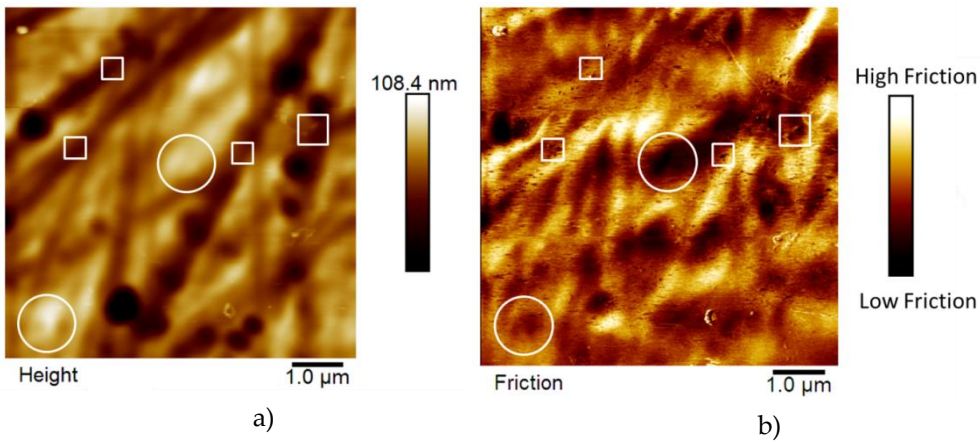

Figure 4.22. AFM measurements on a DLC-coated mesa after run-in. a) Friction force (dark colors correspond to low friction); b) Height map of the same area. White circles point at asperities on (a), which show low lateral force on (b); white squares indicate the corresponding locations and lateral force measured at the nanoscale particles. Scan size $10 \times 10\ \mu m^2$*, line frequency* $0{,}5\ Hz$*. Scan direction from left to right.*

Together with the highest asperities, also the nanoscale particles exhibit a low friction coefficient. This is illustrated by the dark spots in Fig. 4.22a, marked with the white circles. One can see that some of these particles have ended up in the valleys, while others reside in higher regions on the surface. Like the highest asperities, the higher ones are probable to form part of the true contact area and assist in the lubrication process. We assume that, in full analogy with the larger carbon-based particles, investigated in Fig. 4.21, the highest asperities and these nanoscale particles are partially graphitized. Unfortunately, the spot size in our micro-Raman spectroscopy measurements was too large to directly confirm this. The scenario suggested by our observations resembles that of the formation of so-called nanoscrolls, which are thought to have extremely lubricious properties. Berman et al [19] have recently shown that graphene patches can wrap around nanodiamonds. This might significantly lower the sliding friction on DLC, again via the effect of structural lubricity, or superlubricity between graphite surfaces, shown in e.g. [35-37]. Interestingly, some of the low-friction spots if Fig. 4.22a do not correlate with protrusions in Fig. 4.22b. We assume that these are wear sites, where nano-particles have originated under the influence of high shear stresses. Either during the shearing-off process or during subsequent sliding in contact with the opposing surface, these sites may have changed their carbon network structure.

4.4 Summary

Micropatterning of the studied DLC substrates is an essential instrument that helps directly to control an apparent area of contact between the sliding surfaces. As a result, we can observe origin, step-by-step formation and development of third-body elements during the sliding friction on the fixed areas of contact. Our observations suggest that high local stresses lead to the formation of DLC microparticles with increased numbers of sp^2-bonded clusters, which in turn serve as a lubricant. In turn, the microparticles seem later to decompose into nanoparticles, which demonstrate the low friction coefficient too. Adding here the lubrication due to surface transformation at the highest asperities on the DLC, all together it results in lowering of the sliding friction coefficient regardless of the choice of counter sample. We have also shown a correlation between presence and absence of the particle debris from the counter, which take part in the contacting

interface. We suspect that the surface of e.g. Si flakes got wrapped with a thin layer of carbon material transferred from the DLC surface during their initial shear. The last could explain their mobility at the sliding interface. More research is needed to be done on the level of single nano- and microparticles of DLC and counter material in order to relate their surface properties to the low friction coefficient at the macroscopic level they deliver together.

4.5 Bibliography

1. Aksenov, I.I. & Strel'nitskij, V.E. Wear resistance of diamond-like carbon coatings. *Surface and Coatings Technology* **47**, pp. 252-256 (1991)
2. Savvides, N. & Bell, T.J. Hardness and elastic modulus of diamond and diamond-like carbon films. *Thin Solid Films* **228**, pp. 289-292 (1993)
3. Erdemir, A. & Donnet, C. Tribology of diamond-like carbon films: recent progress and future prospects, J. Phys. D: Appl. Phys. **39**, pp. 311-327 (2006)
4. Banerij, A. *et al*. High temperature tribological behavior of W containing diamond-like carbon (DLC) coating against titanium alloys, *Surf. And Coat. Technology* **241**, pp. 93-104 (2014)
5. Yang, B. *et al*. The high temperature tribological properties of Si-DLC films. *Surf. and Interf. Analysis* **13**, pp. 1601-1605 (2012)
6. Erdemir, A. *et al*. Friction and wear performance of diamond like carbon films grown in various source gas plasmas, *Surf. Coat. Technol*. **120-121**, pp. 589-593 (1999)
7. Grill, A.: Diamond-like carbon: state of the art, *Diamond and Related Materials* **8**, pp. 428-434 (1999)
8. Ronkainen *et al*. Friction and wear properties in dry, water- and oil-lubricated DLC against alumina and DLC against steel contacts. *Wear* **222**, pp. 120-128 (1998)
9. Lettington, A. Applications of diamond-like carbon thin films. *Thin Film Diamond* (Elsevier) 1998
10. Wei, Q. *et al*. Mechanical properties of diamond-like carbon composite thin films prepared by pulsed laser deposition. *Composites Part B: Engineering* **30,** 675–684 (1999).
11. Donnet, C. *et* al. The role of hydrogen on the friction mechanism of DLC films. *Tribology Letters* **9**, pp. 137-142 (2000)
12. Eryilmaz, O. L. & Erdemir, A. On the hydrogen lubrication mechanism(s) of DLC films: An imaging TOF-SIMS study. *Surf Coatings Technology* **203**, pp. 750-755 (2008)

13. Hu, L., *et al*. Transformation of sp3 to sp2 sites of diamond like carbon coatings during friction in vacuum and under water vapour environment. *Thin Solid Films* **290**, pp. 126-130 (1996)
14. Marino, M. *et al.* Understanding Run-In Behavior of Diamond-Like Carbon Friction and Preventing Diamond-Like Carbon Wear in Humid Air. *Langmuir* **27**, pp. 12702-12708 (2011).
15. Konicek *et al.* Influence of surface passivation on the friction and wear behavior of ultrananocrystalline diamond and tetrahedral amorphous carbon thin films. *Phys Rev B* **85**, 155448 (2012).
16. Erdemir, A. Genesis of superlow friction and wear in diamondlike carbon films. *Tribology International* **37**, pp. 1005-1012 (2004)
17. Al-Azizi, A. Surface chemistry and Superlubricity of DLC. A Dissertation in Chemical engineering (2016)
18. Hone, J. & Carpick, R. Slippery when dry. *Science* **348**, pp. 1087-1088 (2015)
19. Berman, D. *et al*. Friction. Macroscale superlubricity enabled by graphene nanoscroll formation. *Science* **348**, 1118-22 (2015)
20. Rabinowicz, E. Practical uses of the surface energy criterion Raboniwicz. *Wear* 1964
21. Sutton, D.C. *et al*. The friction of diamond-like carbon coatings in a water environment. *Friction* **1**, pp. 210-221 (2013)
22. Liu, Y. *et al*. An investigation of the relationship between graphitization and frictional behavior of DLC coatings. *Surface and Coatings Technology* **86**, pp. 564-568 (1996)
23. Tai, F.C. *et al*. Multipeak fitting analysis of Raman spectra on DLCH film. *Journal of Raman Spectroscopy* **40**, pp. 1055-1059 (2009)
24. Sadezky, A. Raman microspectroscopy of soot and related carbonaceous materials: Spectral analysis and structural information. *Carbon* **43**, pp. 1731-1742 (2005)
25. Kahn, M. *et al.* Structural and mechanical properties of diamond-like carbon films deposited by an anode layer source. *Thin Solid Films* **517**, pp. 6502-6507 (2009)
26. Casiraghi, C. Raman spectroscopy of hydrogenated amorphous carbons. *Phyicals Review B* **72**, 085401 (2005)

27. Ferrari, A.C. & Robertson, J. Resonant Raman spectroscopy of disordered, amorphous, and diamondlike carbon. *Phys Rev B* **64**, 075414 (2001)
28. Kim, D.-W. & Kim, K.-W. Effects of sliding velocity and ambient temperature on the friction and wear of a boundary-lubricated, multi-layered DLC coating. *Wear* **315**, pp. 95-102 (2014)
29. Scharf, T.W. & Singer, I.L. Quantification of the Thickness of Carbon Transfer Films Using Raman Tribometry. *Tribology Letters* **14**, pp. 137-145 (2003)
30. Erdemir, A. & Eryilmaz, O. Achieving superlubricity in DLC films by controlling bulk, surface, and tribochemistry. *Friction* **2**, pp. 140-155 (2014)
31. Rose, F. *et al.* Complete characterization by Raman spectroscopy of the structural properties of thin hydrogenated diamond-like carbon films exposed to rapid thermal annealing. *Journal of Applied Physics* **116**, 123516 (2014)
32. Romero, P. *et al*. Surface passivation and boundary lubrication of self-mated tetrahedral amorphous carbon asperities under extreme tribological conditions. *Friction* **2**, pp. 123-208 (2014)
33. Kim, S. *et al.* Effects of Humidity on the Friction Coefficient of Diamond-Like Carbon (DLC) Coating. *Journal of Korean Physical Society* **54**, pp. 2212-2218 (2009)
34. Brennan, J. *et al*. Adsorption of Water in Activated Carbons: Effects of Pore Blocking and Connectivity. *Langmuir* **18**, pp. 5438-5447 (2002)
35. Dienwiebel, M. *et al.* Superlubricity of graphite. *Physical Review Letters* **92**, 126101 (2004)
36. Cihan, E. *et al*. Structural lubricity under ambient conditions. *Nature Communications* **7**, 12055 (2016)
37. Feng, X. *et al*. Superlubric Sliding of Graphene Nanoflakes on Graphene. *ACS Nano* **7**, pp. 1718-1724 (2013)
38. Irmer, G. & Dorner-Risel, A. Micro-Raman studies on DLC. *Advanced Engineering Materials* **7**, pp. 694-705 (2005)
39. Hong, S.-H. & Winter, J. Micro-Raman spectroscopy on a-C:H nanoparticles. *Journal of Applied Physics* **98**, 124304 (2005)
40. Ahn, H.-S. *et al.* Application of phase contrast imaging atomic force microscopy to tribofilms on DLC coatings. *Wear* **249**, pp. 617-625 (2001)

41. Hansma, H. *et al.* Properties of biomolecules measured from atomic force microscope images: a review. *Journal of structural biology* **119**, pp. 99-108 (1997)
42. Butt, H.-J. *et al*. Force measurements with the atomic force microscope: technique, interpretation and applications. *Surface Science Reports* **59**, pp. 1-152 (2005)
43. Haugstad, G. & Jones, R. Mechanisms of dynamic force microscopy on polyvinyl alcohol: region-specific non-contact and intermittent contact regimes. *Ultramicroscopy* **76**, pp. 77-86 (1999)
44. Cook, R.F. Strength and sharp contact fracture of silicon. *Journal of Materail Science* **41**, pp. 841-872 (2006)
45. Gustavsson, F. Formation of tribologically beneficial layer on counter surface with smart chemical design of DLC coating in fuel contact. *Tribology - Materials, Surfaces & Interfaces* **6** (2013)
46. Gayathri, S. *et* al. Impact of laser power density on tribological properties of Pulsed Laser Deposited DLC films. *AIP Advances* **3**, 122113 (2013)
47. Zhao, F. Structural, mechanical and tribological characterizations of a-C:H:Si films prepared by a hybrid PECVD and sputtering technique. *Journal of Applied* Physics **42**, 165407 (2009)
48. Si-mat.com/silicon-wafers.html Visited on 05 April 2017
49. Williams, R. & Goodman, A.M. Wetting of thin layers of Si_2O by water. *Applied Physics Letters* **25**, 531 (1974)
50. Ni, W. *et al*. Tribological behavior of diamond-like-carbon (DLC) coatings against aluminum alloys at elevated temperatures. *Surface & Coatings Technology* **201**, pp. 277-283 (2006)
51. Enachescu, M. *et al.* Atomic Force Microscopy Study of a Ideally Hard Contact: The Diamond(111)/Tungsten Carbide Interface. *Physical Review Letters* **88**, pp. 1877-1879 (1998)
52. Li, H. *et al*. Humidity dependence on the friction and wear behavior of diamond-like carbon film in air and nitrogen environments. *Diamond & Related Materials* **15**, pp. 1585-1592 (2006)
53. Song, J. *et al.* Penetration depth at various Raman excitation wavelengths and stress model for Raman spectrum in biaxially-strained Si. *Science China Physics, Mechanics and Astronomy* **56**, pp. 2065-2070 (2013)

54. Kumar, N. *et* al. Super-low to high friction of turbostratic graphite under various atmospheric test conditions. *Tribology International* **44**, pp. 1969-1978 (2011)
55. https://www.vaisala.com/ Visited on 09 April 2017